Use of Model Based Systems Engineering and Development in the Design of a Commercial Nose-Radome Test System Employing a Multi-Axis Cobot

S.F. Gregson[1, 2], D. Lewis[3], P. Schluper[1], G.E. Hindman[1]
[1] Next Phase Measurements LLC, CA, USA, stuart.gregson@qmul.ac.uk
[2] Queen Mary University London, London, UK
[3]Boeing, Seattle, USA

***Abstract*—In most instances antenna test facilities are designed with a specific measurement application in mind. As a result, these facilities tend to be optimised for that task and have fixed measurement geometries. The move towards antenna measurement ranges employing multi-axis industrial robotic positioners that provide a near limitless degree of flexibility in terms of measurement types and scan geometries complicates design and development tasks. The available flexibility and ability to continuously adapt and refine the acquisitions results in an ongoing need to evaluate each unique setup and application. Model based Systems Engineering and Development (MBSE/MBD) techniques can be employed to dramatically reduce the time, cost, and effort of developing and validating new measurement scenarios. This paper illustrates the use of MBSE in the implementation of a new nose-mounted radome test system employing industrial multi-axis robots. In this novel application, a collaborative robot (Cobot) is used to emulate a classical antenna gimbal, requiring extensive use of MBSE to develop and verify the measurement and control sub-systems.**

Index Nose-Mounted, Radome-Test, Collaborative Robot, MBSE, DO-213A, RTCA.

I. INTRODUCTION

The use of Model Based Systems Engineering and Development (MBSE/MBD) approaches have proliferated over recent years and have found great utility in reducing the time, risk, and cost for programme development and validation. This is all the more important with considering systems employing multi-axis industrial robots now used in many modern complex antenna test systems [1]. This has been made possible by the growth in computer processing, which has only recently allowed the three-dimensional full-wave computational electromagnetic (CEM) simulations to emulate realistic free-field measurement systems. This capability, combined with modern computer aided design (CAD) tools, has enabled complex test systems to be visualised long before any hardware becomes available. In this way, MBSE tools can be used to optimise and configure a slew of measurement configurations to explore and evaluate new concepts of operation (ConOps) far earlier within the programme cycle than would otherwise be possible. They can also be used to reduce measurement uncertainties, and to verify and validate processing techniques [1, 2, 3].

Multi-axis robotic systems are generally capable of acquiring classical spherical, cylindrical and planar near-field data, as well as taking extrapolated gain or direct far-field measurements. Additionally, the flexibility provided by such systems allows other types of measurement [4, 5, 6, 7]. The adaptability of the system affords the test engineer unique opportunities to acquire highly accurate, uniquely tailored measurements, that are perhaps not available from other more traditional systems. However, with this flexibility comes the associated difficulty of understanding and optimizing individual modes of operation. This is further compounded when these systems are upgraded with additional capabilities. In this paper we shall illustrate the utility of MBSE techniques by considering the upgrade of a dual robotic antenna measurement system to enable the measurement of nose-mounted commercial radomes. The structure of this paper is as follows. First, we provide a description of the existing dual robotic antenna test system. Next, we illustrate how this can be upgraded to take commercial nose-mounted radome measurements using a collaborative robot (Cobot) to emulate a conventional elevation over azimuth antenna gimbal; followed by implementation of MBSE techniques to develop and validate the antenna pointing and polarization transformations required to undertake classical radome measurements using this novel test system.

II. ROBOTIC ANTENNA MEASUREMENT SYSTEM FACILITY OVERVIEW

A dual six-axis industrial robotic antenna measurement system is considered here, installed within an environmentally controlled 12.5 × 8 × 5 m [41’ × 26’ × 17’] (L x W x H) screened anechoic chamber lined with 0.60 m [24”] pyramidal absorber. Of the two multi-axis industrial robots, one has a fixed base, while the other is installed atop a 9 m [30’] long linear translation stage. The multi-axis robots are each installed on pedestals to raise the AUT and probe towards the centre-line of the chamber. This arrangement can be seen illustrated in Fig. 1 with the stationary robot (SR) shown to the left-hand side of the figure, and the moving robot (MR) located to the right. The system, as shown, provides fourteen separate motion axes which are all under computer control. The two six-axis

robots comprise twelve of the motion axes, the motorized linear stage under the MR robots is the thirteenth axis, and an AUT azimuth stage is the fourteenth axis. This last stage is used as a ϕ-axis of the spherical near-field (SNF) positioning system of the radome test system, not shown in Fig 1.

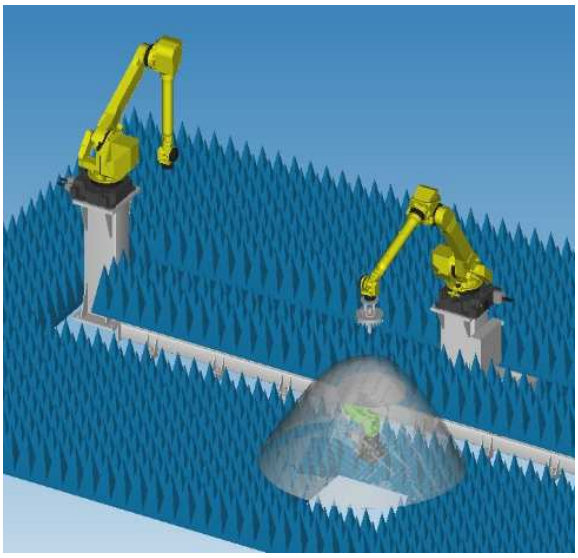

Fig. 1. Illustration of the new dual 6-axis robotic antenna measurement system shown with new nose-radome upgrade.

In Fig. 2 we present a schematic of a commercial nose-mounted radome installed about the six-axis collaborative robot which can be seen placed atop the floor-mounted azimuth stage used as the ϕ-axis of a (θ,ϕ) spherical measurement. Here, the θ motion is provided by the MR to acquire near-field data in an over-head scanning arm configuration, which is a well-known, well-understood spherical acquisition measurement mode [8] for which efficient near-field to far-field transformation algorithms are available.

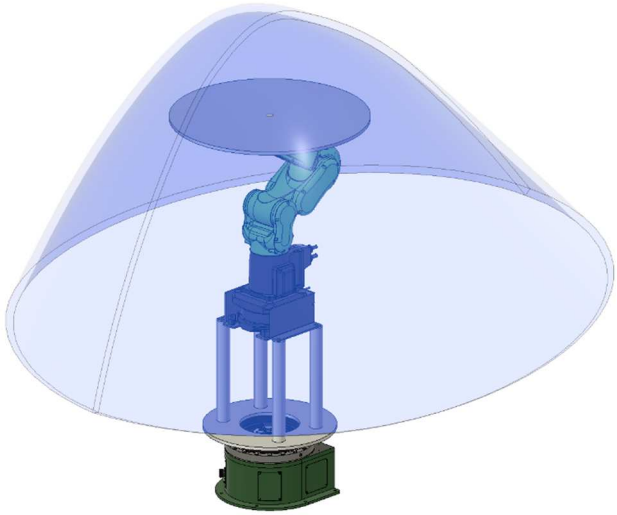

Fig. 2. Illustration of the new 6-axis cobot antenna positioner situated within a commercial nose-mounted radome.

The test requirements for nose-mounted commercial radomes are controlled by the Radio Technical Commission for Aeronautics (RTCA) and are carefully prescribed in references [9], [10], [11]. Specifically, DO-213A provides the minimum operational performance standard for nose-mounted radomes specifications used for evaluating the radome's effects on a weather radar antenna and permits the use of near-field measurement techniques in this evaluation process. The radome measurements specified by this standard require the measurement simulates the actual operation on the airframe. Thus, the antenna positioner should position the radar antenna within a radome to emulate its positioning used in the aircraft installation. Typically, weather radar antennas employ elevation over azimuth gimbals. These positioners provide the mechanical steering of the antenna with the elevation over azimuth (el/az) coordinate system being fixed to the airframe, rather than being fixed to the antenna as is the case with classical antenna measurement coordinate systems, *cf.* [8, 11]. In classical antenna measurements, the reference coordinate system is fixed to the AUT as it is rotated or translated. The reason this reference coordinate system is not fixed in the range coordinate system is because the properties we wish to measure be fixed to the range coordinate system rather than the desired antenna coordinate system. It is important to note that there is thus an alternative point of view that changes the definition of where the polar axis of the coordinate system is located. This alternative definition leads to differences in the associated spherical angles and vector components. Here, we are treating the antenna like a radar, and determining where its main beam is pointed in a coordinate system that is fixed to the range as the theta and phi positioners are rotated. This is the case we are considering here and is the root cause for the differences in the relationship between the azimuth and elevation angles and the direction cosines. In practice, the result of these different definitions is typically small. Along the principal plane cuts there is no difference. However, as one moves off-axis into the intercardinal regions, we see the most significant differences.

In the next section we use these definitions to develop the relationship between the azimuth and elevation airframe gimble angles and the joint rotations required to emulate this in the multi-axis cobot.

III. Overview of the Application of MBSE/MBD

In this section we illustrate the use of MBSE/MBD to determine antenna positioning within a commercial nose-mounted radome by constructing a mathematical model of the system shown in Fig 2 above. To do this, let us first define the requisite coordinate systems. The Range Fixed System (RFS) co-ordinate axes form a right-handed set and is the fixed fiducial system within the facility [8]. This forms the basic reference system in the spherical range. The RFS system is used for the acquisition, *i.e.* tabulation, of the near-field spherical components. The Antenna Mechanical System (AMS) forms a right-handed set nominally orientated

coincident and synonymous with the RFS axes. This is the base system that is used for plotting the far-field patterns. These systems are related by the translations and rotations of the various axes and can be expressed in a linear algebra form by means of a set of matrices that represent an isometric transformation. Passive transformation matrices are matrices that post-multiply a point vector to produce a new point vector and is merely a change in the co-ordinate system. The relationship between two co-ordinate systems can be defined with the use of a four-by-four homogeneous transformation matrix namely [8],

$$\begin{bmatrix} x' \\ y' \\ z' \\ 1 \end{bmatrix} = \begin{bmatrix} A_{1,1} & A_{1,2} & A_{1,3} & A_{1,4} \\ A_{2,1} & A_{2,2} & A_{2,3} & A_{2,4} \\ A_{3,1} & A_{3,2} & A_{3,3} & A_{3,4} \\ 0 & 0 & 0 & 1 \end{bmatrix} \cdot \begin{bmatrix} x \\ y \\ z \\ 1 \end{bmatrix} \tag{1}$$

Here, the elements $A_{1,4}$, $A_{2,4}$ and $A_{3,4}$ represent a translation between the origins of the respective frames of reference. The three-by-three sub matrix,

$$\begin{bmatrix} A_{1,1} & A_{1,2} & A_{1,3} \\ A_{2,1} & A_{2,2} & A_{2,3} \\ A_{3,1} & A_{3,2} & A_{3,3} \end{bmatrix} = \begin{bmatrix} \underline{\hat{e}}_{x'} \cdot \underline{\hat{e}}_x & \underline{\hat{e}}_{x'} \cdot \underline{\hat{e}}_y & \underline{\hat{e}}_{x'} \cdot \underline{\hat{e}}_z \\ \underline{\hat{e}}_{y'} \cdot \underline{\hat{e}}_x & \underline{\hat{e}}_{y'} \cdot \underline{\hat{e}}_y & \underline{\hat{e}}_{y'} \cdot \underline{\hat{e}}_z \\ \underline{\hat{e}}_{z'} \cdot \underline{\hat{e}}_x & \underline{\hat{e}}_{z'} \cdot \underline{\hat{e}}_y & \underline{\hat{e}}_{z'} \cdot \underline{\hat{e}}_z \end{bmatrix} \tag{2}$$

contains the rotational information relating these frames of reference. This can also be expressed in terms of the cosine of the angles between the various combinations of unit vectors. The determinate of this sub matrix can be calculated and any significant deviation from unity can be treated as being indicative of a bad direction cosine matrix. By way of illustration, rotations about the x- and z-axes are represented respectively by the matrices [11] in (3) and (4),

$$R_x = \begin{bmatrix} 1 & 0 & 0 & 0 \\ 0 & \cos\theta_x & \sin\theta_x & 0 \\ 0 & -\sin\theta_x & \cos\theta_x & 0 \\ 0 & 0 & 0 & 1 \end{bmatrix} \tag{3}$$

$$R_z = \begin{bmatrix} \cos\theta_z & \sin\theta_z & 0 & 0 \\ -\sin\theta_z & \cos\theta_z & 0 & 0 \\ 0 & 0 & 1 & 0 \\ 0 & 0 & 0 & 1 \end{bmatrix} \tag{4}$$

The derivation of these rotation matrices can either be obtained from the use of trigonometric identities or from geometry. A series of transformation matrices may be concatenated into a single matrix through matrix multiplication where the order is noncommutative. For the case of the six-axis cobot that is installed upon a phi-axis rotation stage, as shown in Fig. 3, the rotations and translations that describe the position of the AUT are defined as follows: J_0 is the ϕ-axis rotation stage, then J_1 through to J_6 represent the six axes of the cobot starting from the base and moving towards the end effector. Here, J_0 and J_1 are z-axis rotations, J_2 and J_3 are x-axis rotations, J_4 is a further z-axis rotation, J_5 is an x-axis rotation, and finally J_6 is another z-axis rotation. The linear displacements, *i.e.* limb lengths are crucial for positioning the AUT within the radome, however for the purpose of pointing and polarization alignment they are unimportant. For the cobot under consideration here, the lengths, starting at the base of the cobot and moving successively toward the end-effector were: l_1 = 159, l_2 = 260, l_3 = 65, l_4 = 225, l_5 = 69.5 where the dimensions are all in mm. By cascading the rotation and translation matrices together the position and pointing of the AUT can be determined for any given set of rotations. Although laborious, this is not difficult. This enables the relationship between the AMS and RFS to be established for any such robot. This can be seen illustrated in Fig. 3 below.

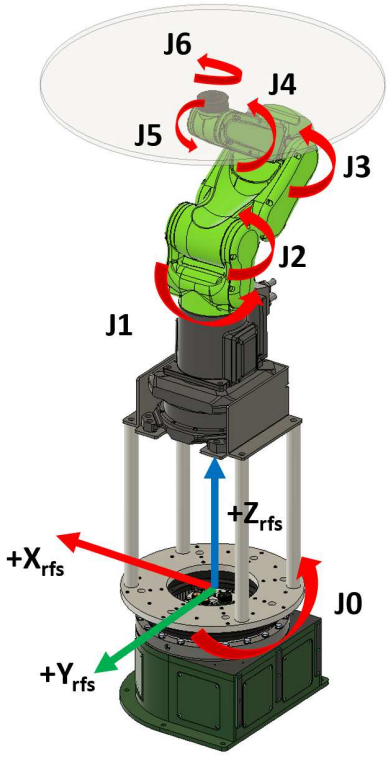

Fig. 3. Illustration of the new 6-axis cobot antenna positioner with each of the rotation axes labelled.

Typically, commercial nose-mounted radome measurements are taken with an aircraft gimbal which is used to mechanically scan the antenna to a series of azimuth and elevation angles where the positioner equates to an elevation over azimuth positioner. As the angles are defined with respect to a fixed coordinate system that is attached to the fuselage, this corresponds to a coordinate system that has poles which align with the ±y-axes. Thus, the direction cosines of a vector defined in this way may be expressed as,

$$u = \sin(Az)\cos(El) \tag{5}$$

$$v = \sin(El) \tag{6}$$

$$w = \cos(Az)\cos(El) \tag{7}$$

The equivalent conventional spherical θ, ϕ angles can be computed using [8],

$$\theta = \arccos(w) \tag{8}$$

$$\phi = \arctan\left(\frac{v}{u}\right) \tag{9}$$

Where it is understood that "arctan" denotes the four-quadrant arctangent function. We may therefore command the cobot to point the AUT in the desired azimuth and elevation direction by setting J_1 equal to ϕ, and utilizing the J_5 axis to steer in theta. Here however the J_5 axis angle will need to be adapted by J_3 where J_3 is set by an angle that is required to centre J_5 directly above J_1. Although it can be seen that this correctly points the AUT in the desired direction as determined by the azimuth and elevation angles, the question of antenna rotation about this direction, and the impact that this has upon polarization still needs to be addressed. The elevation over azimuth mechanical steering has an accompanying linear polarization definition. If measurements made using the cobot are to be compared with those taken using other conventional radome test facilities, then this must be accounted for within the antenna alignment. Fortunately, we can utilize J_6 for this purpose. Once set, we may add one further 90° rotation to allow measurements to be taken with the antenna nominally for either H-pol, or V-pol.

We shall now develop expressions that can be used to determine this J_6 rotation. We may determine the additional J_6 rotation angle from knowledge of the AMS z-axis and AUT x-axis when known in the RFS, *cf.* (2). This we have at hand as we can use the chained direction cosine matrices derived above to transform a unit vector in the x-axis and y-axis to the RFS. With these vectors we may deduce the desired tilt angle. Here, we let $\underline{\hat{n}}$ be a unit normal to the antenna aperture plane, this is the Z_{AMS} unit vector. Let $\underline{P}$ be orthogonal to $\underline{\hat{n}}$ and the y_{RFS}, and therefore resides within the RFS xz-plane. Let $\underline{q}$ be orthogonal to both $\underline{P}$ and $\underline{\hat{n}}$, and $\underline{v}_T$ be the top edge vector, which is x_{AMS} unit vector. We may then express these vectors (where x, y, z are all in the RFS) as,

$$\underline{p} = \underline{n} \times \underline{\hat{y}} = \begin{vmatrix} \underline{\hat{x}} & \underline{\hat{y}} & \underline{\hat{z}} \\ n_x & n_y & n_z \\ 0 & 1 & 0 \end{vmatrix} \tag{10}$$

And,

$$\underline{q} = \underline{p} \times \underline{n} = \begin{vmatrix} \underline{\hat{x}} & \underline{\hat{y}} & \underline{\hat{z}} \\ -n_z & 0 & n_x \\ n_x & n_y & n_z \end{vmatrix} \tag{11}$$

Where $\underline{\hat{n}}$ is a unit normal to the aperture. Thus, we may deduce the necessary roll angle correction from,

$$\text{roll} = \sin^{-1}\left(\frac{\underline{q} \cdot \underline{v}_t}{|\underline{q}||\underline{v}_t|}\right) \tag{12}$$

Care needs to be taken to ensure that the length of each of these vectors is correctly normalized to unity as the cross-product operation does not automatically guarantee this. In this way, we can determine the requisite J_6 offset angle which means we may correctly orientate the AUT to the desired polarization definition.

Figure 4 presents an illustration of the mathematical model that was developed above. Here, we have also included the x-, y-, and z-axis unit vectors for the AMS and RFS coordinate system respectively together with a rendering of the weather radar, the multi-axis cobot, the spherical range phi-axis, and the elevation over azimuth airframe gimbal coordinate system and lattice of specified measurement positions. This set of directions are represented by the red dots in Figures 4, 5, and 6. Here, these locations are defined by the RTCA specification document which specifies a grid of points that spans ±90° in azimuth in 10° increments, and ±25° elevation in 5° increments. In each of these figures we see the AMS z-axis pointing at one of these dots indicating that the weather radar has been mechanically steered to the correct direction. Although not possible to show in a paper, the model shown in Fig. 4 can be animated so that the observer can see the radar rotate which was enormously valuable in the verification and validation of the mathematical model developed above. This is a very powerful illustration of the practical value of MBSE.

Having established that the weather radar has been commanded to point in the correct direction, further verification of the rotational orientation of the antenna was desired. We examine this in greater detail in Fig. 5 where we show the system in plan-view.

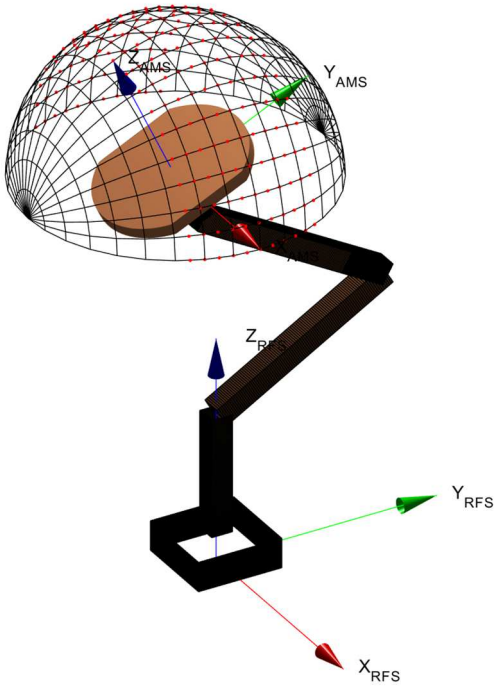

Fig. 4. Illustration of the new 6-axis cobot antenna positioner shown in relation to the range fixed coordinate system together with the antenna mechanical coordinate system.

By way of further verification Fig. 5 shows the system in plan-view for the H-pol case, and Fig. 6 for the V-pol AUT orientated case where the six-axis cobot has been used to emulate the airframe elevation over azimuth gimbal.

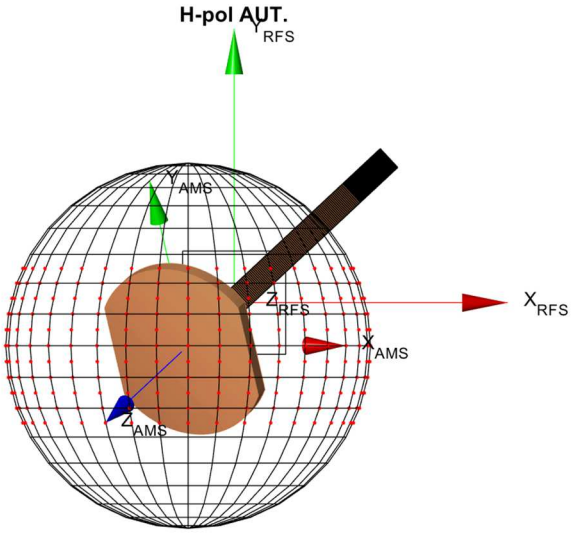

Fig. 5. Plan-view schematic of the AUT when orientated to be H-pol in the RFS.

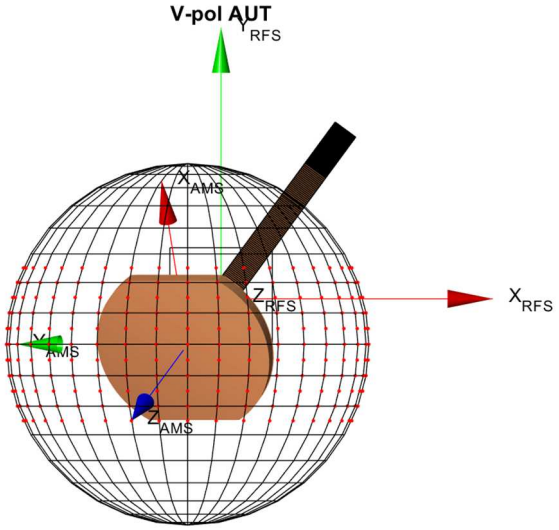

Fig. 6. Plan-view schematic of the AUT when orientated to be V-pol in the RFS.

IV. Summary and Conclusions

This paper presents an overview of a new, novel, nose-mounted commercial radome test system that utilises an existing dual robotic antenna measurement system and a six-axis collaborative robot which is used to emulate conventional elevation over azimuth gimbals to position a thirty-inch x-band weather radar behind the radome. The alignment transformation between the range fixed coordinate system and the antenna mechanical coordinate system is derived while also taking account of the necessary polarisation alignment. The development and verification of these transformations are established by using MBSE concepts to create a dynamic model of the system that enabled rapid and clear verification of the necessary transformations required for all radar scan angles and prototyped a new triple robotic antenna measurement system (TRAMS).

References

[1] J.A. Estefan, “Survey of model-based systems engineering (MBSE) methodologies.”, Incose MBSE Focus Group 25 (2007)

[2] M. Grieves, “Digital Twin: Manufacturing Excellence through Virtual Factory Replication”, 2015.

[3] D.M. Lewis, J. Bommer, G.E. Hindman, S.F. Gregson, "Traditional to modern antenna test environments: The impact of robotics and computational electromagnetic simulation on modern antenna measurements," 15th European Conference on Antennas and Propagation (EuCAP), 2021

[4] D. Novotny, et al, “Performance evaluation of a robotically controlled millimeter-wave near-field pattern range at the NIST”, 2013 7th European Conference on Antennas and Propagation

[5] J. Guerrieri, et al, “Configurable Robotic Millimeter-Wave Antenna Facility”, 2015 9th European Conference on Antennas and Propagation

[6] J Guerrieri, et al, “Validation of Robotics for Antenna Measurements”, 2017 11th European Conference on Antennas and Propagation

[7] D. R. Novotny, J. A. Gordon, M. S. Allman, “The Multi-Robot Large Antenna Positioning System for Over- The-Air Testing at the National Institute of Standards and Technology”, Proceedings of the AMTA Symposium.

[8] C.G. Parini, S.F. Gregson, J. McCormick, D. Janse van Rensburg, T. Eibert, “Theory and Practice of Modern Antenna Range Measurements 2nd Expanded Edition, Volume 1”, IET Electromagnetic Waves series 55 ISBN 978-1-83953-126-2, 2021.

[9] RTCA SC-173, "Change No. 1 to RTCA/DO-213 Minimum Operational Performance Standards For Nose-Mounted Radomes" RTCA, Inc., www.rtca.org, 1995.

[10] RTCA SC-230, "RTCA/DO-220A, Minimum Operational Performance Standards (MOPS) for Airborne Weather Radar Systems”, RTCA, Inc., www.rtca.org, 2016.

[11] RTCA SC-230, "RTCA/DO-213A Minimum Operational Performance Standards For Nose-Mounted Radomes," RTCA, Inc., www.rtca.org, 2016.